PHYSICAL REVIEW D **92,** 043509 (2015)

Planck trispectrum constraints on primordial non-Gaussianity at cubic order

Chang Feng,[1,*] Asantha Cooray,[1] Joseph Smidt,[2] Jon O'Bryan,[1] Brian Keating,[3] and Donough Regan[4]

[1]*Department of Physics and Astronomy, University of California, Irvine, California 92697, USA*
[2]*XTD-IDA, Los Alamos National Laboratory, Los Alamos, New Mexico 87545, USA*
[3]*Department of Physics, University of California, San Diego, California 92093-0424, USA*
[4]*Astronomy Centre, University of Sussex, Falmer, Brighton BN1 9QH, United Kingdom*

(Received 2 February 2015; published 6 August 2015)

Non-Gaussianity of the primordial density perturbations provides an important measure to constrain models of inflation. At cubic order the non-Gaussianity is captured by two parameters $\tau_{\rm NL}$ and $g_{\rm NL}$ that determine the amplitude of the density perturbation trispectrum. Here we report measurements of the kurtosis power spectra of the cosmic microwave background temperature as mapped by Planck by making use of correlations between square temperature-square temperature and cubic temperature-temperature anisotropies. In combination with noise simulations, we find the best joint estimates to be $\tau_{\rm NL} = 0.4 \pm 0.9 \times 10^4$ and $g_{\rm NL} = -1.2 \pm 2.8 \times 10^5$. If $\tau_{\rm NL} = 0$, we find $g_{\rm NL} = -1.4 \pm 1.8 \times 10^5$.

DOI: 10.1103/PhysRevD.92.043509 PACS numbers: 98.80.Es, 95.85.Bh, 98.70.Vc

I. INTRODUCTION

Existing cosmological data from cosmic microwave background (CMB) and large-scale structure are fully consistent with a simple cosmological model involving six basic parameters describing the energy density components of the Universe, age, and the amplitude and spectral index of initial perturbations. The perturbations depart from a scale-free power spectrum and are Gaussian. These facts support inflation as the leading paradigm related to the origin of density perturbations [1–3]. Under inflation a nearly exponential expansion stretched space in the first moments of the early Universe and promoted microscopic quantum fluctuations to perturbations on cosmological scales today [4,5]. Moving beyond simple inflationary models with a single scalar field, models of inflation now involve multiple fields and exotic objects such as branes that have nontrivial interactions. Such inflationary models produce a departure from Gaussianity in a model-dependent manner [6–9]. The amplitude of non-Gaussianity therefore is an important cosmological parameter that can distinguish between the plethora of inflationary models [10].

The value of the first-order non-Gaussian parameter, $f_{\rm NL}$, has been obtained with increasing success using the bispectrum—the Fourier analog of the three-point correlation function of the CMB temperature. Such studies have found $f_{\rm NL}$ to be consistent with zero [11–14], with the strongest constraint coming from Planck given by $f_{\rm NL} = 2.7 \pm 5.8$ [15]. The single-field, slow-roll inflationary model expectation is that $f_{\rm NL} \lesssim 1$ and a constraint at such a low-amplitude level may be feasible in the future with large-scale structure data and with 21-cm intensity fluctuations. Alternatively, with the trispectrum or four-point correlation function of CMB anisotropies [16], we can measure the second- and third-order non-Gaussian parameters $\tau_{\rm NL}$ and $g_{\rm NL}$. While these higher-order parameters generally lead to a trispectrum that has a lower signal-to-noise ratio than the bispectrum, there may be models in which the situation is reversed with the trispectrum dominating over the bispectrum contribution. An example of such a model is an inhomogeneous end to thermal inflation discussed in Ref. [17].

A previous analysis using Wilkinson Microwave Anisotropy Probe (WMAP) data out to multipole $\ell < 600$ using the kurtosis power spectra involving two-to-two and three-to-one temperature correlations [18,19], found $-7.4 < g_{\rm NL}/10^5 < 8.2$ and $-0.6 < \tau_{\rm NL}/10^4 < 3.3$ at the 95% C.L. Other measures of the WMAP trispectrum have been presented in Refs. [20–23]. While the Planck data have been used to constrain $\tau_{\rm NL} < 2800$ at the 95% C.L. such a constraint ignored the signal associated with $g_{\rm NL}$ [15]. Using all of the Planck data, the expectation is that $g_{\rm NL}$ can be constrained with a 68% C.L. uncertainty of 6.7×10^4 [21] with $\tau_{\rm NL} = 0$, while $\tau_{\rm NL}$ can be constrained down to 560 if $g_{\rm NL} = 0$ [24]. Here we present an analysis of the Planck temperature anisotropy maps by making use of kurtosis power spectra to constrain $\tau_{\rm NL}$ and $g_{\rm NL}$ jointly.

II. THEORY

We begin the discussion with the temperature trispectrum defined as [25]

$$\langle a_{l_1 m_1} a_{l_2 m_2} a_{l_3 m_3} a_{l_4 m_4} \rangle = \sum_{LM} (-1)^M \begin{pmatrix} l_1 & l_2 & L \\ m_1 & m_2 & -M \end{pmatrix} \times \begin{pmatrix} l_3 & l_4 & L \\ m_3 & m_4 & M \end{pmatrix} T^{l_1 l_2}_{l_3 l_4}(L), \quad (1)$$

*chang.feng@uci.edu

where we have introduced the Wigner 3-j symbol. The angular trispectrum, $T^{l_1 l_2}_{l_3 l_4}(L)$, can be further expressed in terms of sums of the products of Wigner 3-j or 6-j symbols times the so-called reduced trispectrum, $\mathcal{T}^{l_1 l_2}_{l_3 l_4}(L)$. The full trispectrum contains permutations of the reduced trispectrum which are associated with Wigner 6-j symbols [16]

$$T^{l_1 l_2}_{l_3 l_4}(L) = P^{l_1 l_2}_{l_3 l_4}(L) + (2L+1)\sum_{L'}\left[(-1)^{l_2+l_3}\begin{Bmatrix} l_1 & l_2 & L \\ l_4 & l_3 & L' \end{Bmatrix} P^{l_1 l_3}_{l_2 l_4}(L') + (-1)^{L+L'}\begin{Bmatrix} l_1 & l_2 & L \\ l_3 & l_4 & L' \end{Bmatrix} P^{l_1 l_4}_{l_3 l_2}(L')\right], \tag{2}$$

where

$$P^{l_1 l_2}_{l_3 l_4} = \mathcal{T}^{l_1 l_2}_{l_3 l_4} + (-1)^{\Sigma_U}\mathcal{T}^{l_2 l_1}_{l_3 l_4} + (-1)^{\Sigma_L}\mathcal{T}^{l_1 l_2}_{l_4 l_3} + (-1)^{\Sigma_U+\Sigma_L}\mathcal{T}^{l_2 l_1}_{l_4 l_3}, \tag{3}$$

and $\Sigma_U = l_1 + l_2 + L$ and $\Sigma_L = l_3 + l_4 + L$.

To derive the angular trispectrum given by $T^{l_1 l_2}_{l_3 l_4}(L)$ we assume that the curvature perturbations ζ of the Universe generated by inflation follow as

$$\Phi(\mathbf{x}) = \Phi_G(\mathbf{x}) + f_{\rm NL}(\Phi^2_G(\mathbf{x}) - \langle\Phi^2_G(\mathbf{x})\rangle) + g_{\rm NL}\Phi^3_G(\mathbf{x}) \tag{4}$$

where the curvature perturbation ζ and the initial gravitational potential are related by $\Phi = (3/5)\zeta$ and $\tau_{\rm NL} = (6f_{\rm NL}/5)^2$.

We refer the reader to Ref. [24] for intermediate steps in our derivation. Using the above form the full trispectrum can be reduced to two forms involving the two amplitudes $\tau_{\rm NL}$ (associated with the $\Phi^2_G(\mathbf{x}) - \langle\Phi^2_G(\mathbf{x})\rangle$ term in the above) and $g_{\rm NL}$ coming from $\Phi^3_G(\mathbf{x})$.

Defining $\mathcal{T}^{l_1 l_2,(i)}_{l_3 l_4}(L) = h_{l_1 l_2 L} h_{l_3 l_4 L} t^{l_1 l_2,(i)}_{l_3 l_4}(L)$, $i = 1, 2$ [26], where

$$h_{l_1 l_2 l_3} = \sqrt{\frac{(2l_1+1)(2l_2+1)(2l_3+1)}{4\pi}}\begin{pmatrix} l_1 & l_2 & l_3 \\ 0 & 0 & 0 \end{pmatrix}, \tag{5}$$

we find that the reduced trispectrum is

$$\mathcal{T}^{l_1 l_2}_{l_3 l_4}(L) = [\tau_{\rm NL}\mathcal{T}^{l_1 l_2,(1)}_{l_3 l_4}(L) + g_{\rm NL}\mathcal{T}^{l_1 l_2,(2)}_{l_3 l_4}(L)]. \tag{6}$$

The two terms are

$$t^{l_1 l_2,(1)}_{l_3 l_4}(L) = \tau_{\rm NL}\left(\frac{5}{3}\right)^2\int r_1^2 dr_1 r_2^2 dr_2 F_L(r_1, r_2) \times \alpha_{l_1}(r_1)\beta_{l_2}(r_1)\alpha_{l_3}(r_2)\beta_{l_4}(r_2), \tag{7}$$

and

$$t^{l_1 l_2,(2)}_{l_3 l_4}(L) = g_{\rm NL}\int r^2 dr \beta_{l_2}(r)\beta_{l_4}(r)[\alpha_{l_1}(r)\beta_{l_3}(r) + \alpha_{l_3}(r)\beta_{l_1}(r)]. \tag{8}$$

Here $\alpha_l(r) = (2/\pi)\int k^2 dk \Delta^{\rm TT}_l(k) j_l(kr)$ and $\beta_l(r) = (2/\pi)\int k^2 dk P(k)\Delta^{\rm TT}_l(k) j_l(kr)$. The primordial curvature power spectrum is $k^3 P(k)/(2\pi^2) = (3/5)^2 A_s (k/k_0)^{n_s - 1}$ with no "running" [27]. Here k_0 is the pivot scale set at 0.05 Mpc^{-1}. We use the public code [28] to compute $\alpha_l(r)$, $\beta_l(r)$ and the temperature transfer function $\Delta^{\rm TT}_l(k)$.

In the $\tau_{\rm NL}$ part, we define the function F_L as

$$F_L(r_1, r_2) = \frac{2}{\pi}\int k^2 dk P(k) j_L(kr_1) j_L(kr_2). \tag{9}$$

Following the efficient algorithm in Ref. [29], we define $\xi = r_2/r_1$, $x = kr_1$ and compress r_1 and r_2 into one dimension such that

$$F_L(\xi) = \frac{2}{\pi} r_1^{1-n_s}\lambda\int dx x^{n_s-2} j_L(x) j_L(\xi x). \tag{10}$$

Here $\lambda = (3/5)^2(2\pi^2/k_0^3)A_s k_0^{4-n_s}$. The integration is performed in the range $x \in [0, 10^5]$. We validate that this fast algorithm gives the same results as Eq. (9).

The first part of the trispectrum associated with $\tau_{\rm NL}$ approximates to $(5/3)^2 C_L^{r_*}\sqrt{C_{l_1}C_{l_2}C_{l_3}C_{l_4}}$ at $L < 100$. This is due to the fact that the integrand peaks at $r = r_*$ and $C_l = \int r^2 dr \alpha_l(r)\beta_l(r)$ [30]. Here r_* is the comoving distance at last scattering surface and $C_L^{r_*} = F_L(r_*, r_*)$. For the comparison with the data, however, we perform an exact calculation defined in Eqs. (7) and (8). The adaptive r grid is used for the integration.

The estimators of the connected trispectrum are constructed in Refs. [19,31] and they are given by

$$K^{(2,2)}_L(\tau_{\rm NL}, g_{\rm NL}) = \frac{1}{2L+1}\sum_{l_1 l_2 l_3 l_4}\frac{1}{2L+1}\frac{\mathcal{T}^{l_1 l_2}_{l_3 l_4}(L)\hat{T}^{l_1 l_2}_{l_3 l_4}(L)}{C_{l_1}C_{l_2}C_{l_3}C_{l_4}}, \tag{11}$$

and

$$K^{(3,1)}_{l_4}(\tau_{\rm NL}, g_{\rm NL}) = \frac{1}{2l_4+1}\sum_{l_1 l_2 l_3 L}\frac{1}{2L+1}\frac{\mathcal{T}^{l_1 l_2}_{l_3 l_4}(L)\hat{T}^{l_1 l_2}_{l_3 l_4}(L)}{C_{l_1}C_{l_2}C_{l_3}C_{l_4}}. \tag{12}$$

In Eqs. (11) and (12), the reduced trispectrum $\mathcal{T}^{l_1 l_2}_{l_3 l_4}(L)$ is evaluated at $\tau_{\rm NL}=1$ and $g_{\rm NL}=1$. The estimators $K_L^{(2,2)}$ and $K_L^{(3,1)}$ are parametrized by these two parameters. The $\hat{T}^{l_1 l_2}_{l_3 l_4}(L)$ denotes the full trispectrum from data or simulation.

In our analysis, $l_{\rm min}\le l_1,l_2,l_3,L\le l_{\rm max}$, $l_{\rm min}=2$ and $l_{\rm max}=1000$. The trispectrum computing time is proportional to $\mathcal{O}(l^4_{\rm max})$ at a single L. In order to make these calculations more efficient, we use Monte Carlo integration for $K_L^{(2,2)}$, i.e., replacing $\sum_{l_1=l_{\rm min}}^{l_{\rm max}}\sum_{l_2=l_{\rm min}}^{l_{\rm max}}\sum_{l_3=l_{\rm min}}^{l_{\rm max}}\sum_{l_4=l_{\rm min}}^{l_{\rm max}}$ by $V/N_{\rm samples}\sum_{\mathbf{l}}$. The vector $\mathbf{l}(=l_1,l_2,l_3,l_4)$ is uniformly sampled from $[l_{\rm min},l_{\rm max}]^4$ and $V=(l_{\rm max}-l_{\rm min})^4$. For $K_L^{(3,1)}$, we restrict the diagonal elements within $2\le L\le 20$ and validate that a bigger upper bound negligibly modifies the trispectrum. The Wigner 3-j symbols' intrinsic selection rule also helps reduce the computation time. With all these efficient algorithms, we can achieve an hour-level computation time, which is about 3 orders of magnitude faster than the brute-force calculation. We show the theoretical predictions of these estimators for the case in Fig. 1 for a fixed set of $\tau_{\rm NL}$ and $g_{\rm NL}$ values for which non-Gaussian simulated maps are available.

From simulated and real data, spherical harmonic coefficients $a_{lm}^{(\rm sim)}$ and $a_{lm}^{(\rm data)}$ are computed by inverse spherical harmonic transformation. Then the two weighted maps are generated from the definitions $A(r,\mathbf{n})=\sum_{lm}\alpha_l(r)\tilde{a}_{lm}Y_{lm}(\mathbf{n})$, $B(r,\mathbf{n})=\sum_{lm}\beta_l(r)\tilde{a}_{lm}Y_{lm}(\mathbf{n})$ and $\tilde{a}_{lm}=a_{lm}/C_l$ where the angular power spectrum C_l is inclusive of noise. $a_{lm}^{(\rm data)}$ is calculated by *anafast* of Healpix which removes the monopole and dipole. To correct the masking effect, we scale the masked modes $a_{lm}^{(\rm sim)}$ and $a_{lm}^{(\rm data)}$ by $1/\sqrt{f_{\rm sky}}$ to match the underlying temperature power spectrum. These masked modes are also beam- and pixel-window-deconvolved. In the following text, we neglect "$\mathbf{n}$" for brevity.

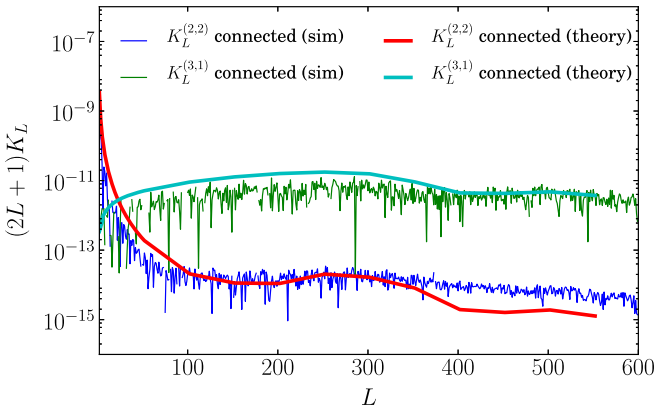

FIG. 1 (color online). The estimator validation using WMAP simulations with $\tau_{\rm NL}=3600$.

From A and B maps, we construct $C(r_1,r_2)=A(r_1)B(r_2)$. Then we make $C'_{lm}=F_L(r_1,r_2)C_{lm}(r_1,r_2)$ and $D(r_1,r_2)=C'(r_1,r_2)A(r_2)$. Here $C_{lm}(r_1,r_2)=\int d\mathbf{n}Y^*_{lm}(\mathbf{n})C(r_1,r_2,\mathbf{n})$. We can calculate four types of power spectra:

$$J_l^{\rm ABA,B}(r_1,r_2)=\frac{1}{2l+1}\sum_m D_{lm}(r_1,r_2)B^*_{lm}(r_2), \tag{13}$$

$$J_l^{\rm AB,AB}(r_1,r_2)=\frac{1}{2l+1}\sum_m F_l(r_1,r_2)[AB]_{lm}(r_1)[AB]^*_{lm}(r_2), \tag{14}$$

$$L_l^{\rm ABB,B}(r)=\frac{1}{2l+1}\sum_m [ABB]_{lm}(r)B^*_{lm}(r), \tag{15}$$

and

$$L_l^{\rm AB,BB}(r)=\frac{1}{2l+1}\sum_m [AB]_{lm}(r)[BB]^*_{lm}(r). \tag{16}$$

When all the power spectra are integrated along the line of sight, they become

$$J_l^{\rm ABA,B}=\int r_1^2dr_1r_2^2dr_2J_l^{\rm ABA,B}(r_1,r_2), \tag{17}$$

$$L_l^{\rm ABB,B}=\int r^2drL_l^{\rm ABB,B}(r), \tag{18}$$

$$J_l^{\rm AB,AB}=\int r_1^2dr_1r_2^2dr_2J_l^{\rm AB,AB}(r_1,r_2), \tag{19}$$

and

$$L_l^{\rm AB,BB}=\int r^2drL_l^{\rm AB,BB}(r). \tag{20}$$

The trispectrum estimators

$$K_L^{(2,2)}=\left(\frac{5}{3}\right)^2J_L^{\rm AB,AB}+2L_L^{\rm AB,BB}, \tag{21}$$

and

$$K_L^{(3,1)}=\left(\frac{5}{3}\right)^2J_L^{\rm ABA,B}+2L_L^{\rm ABB,B} \tag{22}$$

are then constructed from the correlations associated with A and B maps that are either from data or simulations.

These estimators are applied to 143 and 217 GHz temperature data sets, as well as the cross correlation 143×217 GHz. For the cross correlation, the estimators are

$$K_L^{(2,2)}(143\times217) = \left(\frac{5}{3}\right)^2 J_L^{\mathrm{A(143)B(217),A(143)B(217)}} + 2L_L^{\mathrm{A(143)B(217),B(143)B(217)}}, \quad (23)$$

and

$$K_L^{(3,1)}(143\times217) = \left(\frac{5}{3}\right)^2 J_L^{\mathrm{A(143)B(217)A(143),B(217)}} + 2L_L^{\mathrm{A(143)B(217)B(143),B(217)}}. \quad (24)$$

III. SIMULATION VALIDATION

To validate our estimates of the connected trispectra, we make non-Gaussian CMB signal simulations. The non-Gaussian maps for WMAP are publicly available [32] so we simulate maps with $n_{\rm side}=512$ and $l_{\rm max}=600$, and all the WMAP experimental settings, consistent with 5-year observations, are adopted. For the signal part, $a_{lm}=a_{lm}^{\rm G}+f_{\rm NL}a_{lm}^{\rm NG}$ and we choose $f_{\rm NL}=50$, i.e., $\tau_{\rm NL}=3600$ given the expected relation between $f_{\rm NL}$ and $\tau_{\rm NL}$, independent of the exact value of $g_{\rm NL}$. Note that the non-Gaussian simulations we use assume $g_{\rm NL}=0$ and in a joint model fit to data we test this expectation. The WMAP 5-year noises are then added in the signal simulations. The WMAP simulation is $T(\mathbf{n})=\sum_{lm}b_lp_la_{lm}Y_{lm}(\mathbf{n})+\sigma_0/\sqrt{N(\mathbf{n})}n_{\rm white}(\mathbf{n})$. Here σ_0 is the noise per observation and $N(\mathbf{n})$ is the number of observations per pixel. Both σ_0 and $N(\mathbf{n})$ are provided by WMAP. The estimator of the connected trispectrum is $\hat{K}_L=1/4!(K_L-K_L^{\rm Gaussian})$. In Fig. 1 we show that the average connected parts from 100 full-sky realizations are consistent with the theoretical calculations.

IV. DATA ANALYSIS AND RESULTS

We use 2013 Planck 143 and 217 GHz temperature maps for the present analysis. We use the foreground mask to remove the point sources and Galactic emissions for both frequencies. The 217 GHz map cleaned after the 70% foreground mask still contains visible emission around the Galactic plane, so we use an extended mask to further cut the 217 GHz data around it. The resulting sky fractions for both maps become 73% and 58%. At 143 GHz, the map is convolved with a $7'$ Gaussian beam and has 45 μK arcmin noise. At 217 GHz, it is $5'$ and 60 μK arcmin. Following Ref. [33], point sources (PS) and cosmic infrared background (CIB) are also included in simulated data. The power spectra for these two sources are $C_l^{\rm PS}=2\pi/3000^2$ and $C_l^{\rm CIB}=2\pi/(l(l+1))(l/3000)^{0.8}$, respectively. The foreground power at these frequencies are $C_l^{A\times B}=A_{A\times B}^{\rm PS}C_l^{\rm PS}+A_{A\times B}^{\rm CIB}C_l^{\rm CIB}$ with the parameters $A_{143\times143}^{\rm PS}=64\mu{\rm K}^2$, $A_{143\times217}^{\rm PS}=43\mu{\rm K}^2$, $A_{217\times217}^{\rm PS}=57\ \mu{\rm K}^2$, $A_{143\times143}^{\rm CIB}=4\mu{\rm K}^2$, $A_{143\times217}^{\rm CIB}=14\ \mu{\rm K}^2$, $A_{217\times217}^{\rm CIB}=54\ \mu{\rm K}^2$. In addition, a 10 μK arcmin white noise is added into the simulations. The data structure is expressed as $T(\mathbf{n})=\sum_{lm}a_{lm}b_lp_lY_{lm}(\mathbf{n})+n(\mathbf{n})$ where $\mathbf{n}$ is a direction on the sky, b_l is the beam transfer function, p_l is the pixel transfer function at $n_{\rm side}=2048$, and $n(\mathbf{n})$ is the noise simulation. We use 100 signal and noise realizations from the FFP6 simulation set of the Planck Collaboration [34]. We use the best-fit cosmological parameters from "Planck + WP + highL" [27]. Specifically, $\Omega_bh^2=0.022069$, $\Omega_ch^2=0.12025$, $\tau=0.0927$, $n_s=0.9582$, $A_s=2.21071\times10^{-9}$ at pivot scale $k_0=0.05\ {\rm Mpc}^{-1}$, and $H_0=67.15\,{\rm kms}^{-1}{\rm Mpc}^{-1}$ [27].

We calculate both trispectra $K_L^{(2,2)}$ and $K_L^{(3,1)}$ from Gaussian simulations and data for Planck. The Gaussian term in the trispectra $K_L^{\rm Gaussian}$ is averaged from 100 Planck simulations for the frequency combinations 143×143, 143×217 and 217×217 GHz, and is removed from the raw signal, which is defined as the combination of the connected part and the disconnected part. All the trispectra are shown in Fig. 2. It is seen that the disconnected components dominate the raw signal and our simulations can precisely recover these significant biases. Also, all the trispectra show consistent shapes. From 100 simulations, the full covariance matrix $\mathbf{M}$ is obtained for each frequency

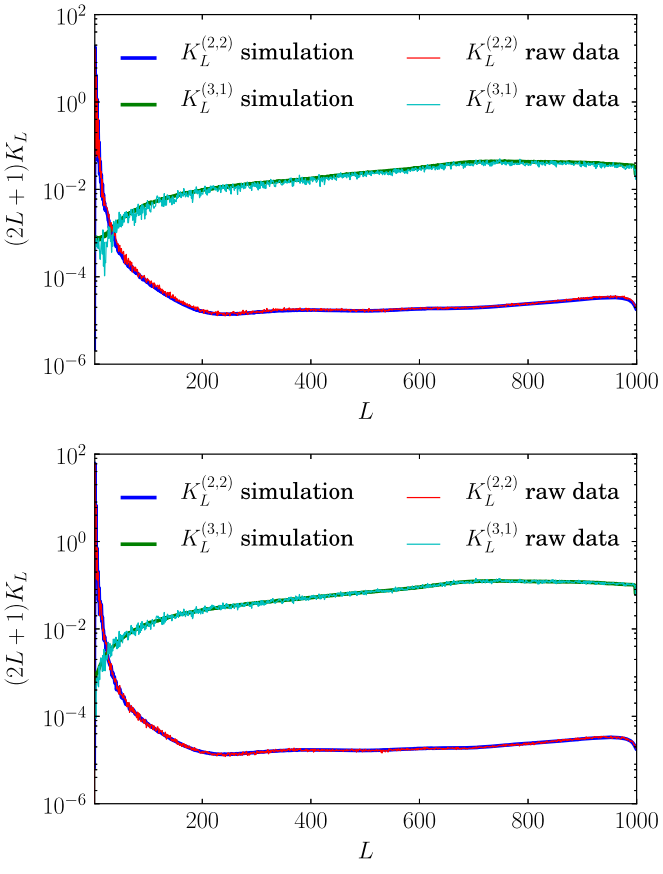

FIG. 2 (color online). The raw trispectra calculated from Planck data and simulations for 143×143 (top) and 143×217 GHz (bottom). In both plots Gaussian bias dominates the raw signal.

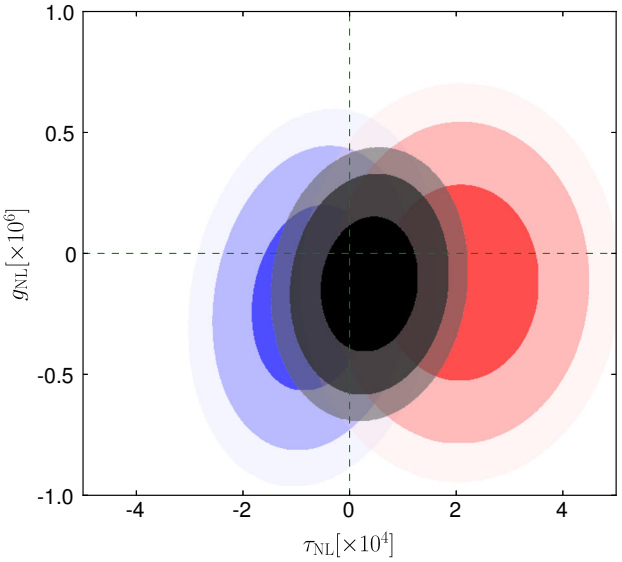

FIG. 3 (color online). The 68%, 95% and 99% confidence levels for different combinations are indicated by the transparency of the contours. The frequency combinations 143×143, 143×217 and $143 \times 143 + 143 \times 217$ GHz are shown in blue, red and black colors.

combination and the vector $V_b = (V_b^{(2,2)}, V_b^{(3,1)})$. Here b is the index of the trispectrum band. We choose five bands for each spectrum: $L = [2, 152]$, [152,302], [302,452], [452,602], [602,800]. Here we use $\Delta L = 150$ and $L_{\rm cut} = 800$. We want to both avoid systematic issues with the high L trispectra and get enough signal to noise, so we choose this conservative cut here.

We choose a binning function to maximize the sensitivity

$$\hat{V}_b = \sum_{L\in b} w_{bL}\hat{S}_L = \frac{\sum_{L\in b} S_L \hat{S}_L/N_L^2}{\sum_{L\in b} S_L^2/N_L^2}, \tag{25}$$

where $S_L = (2L+1)K_L$ is the fiducial model with $\tau_{\rm NL} = g_{\rm NL} = 1$, $N_L = (2L+1)K_L^{\rm Gaussian}$ and $\hat{S}_L = (2L+1)\hat{K}_L$ which is the connected trispectrum from the simulation or data.

The likelihood function of the data is given as

$$\chi^2(\tau_{\rm NL}, g_{\rm NL}) = \sum_{\nu}\sum_{bb'}(V_b^{(\nu)} - \hat{V}_b^{(\nu)})M_{bb'}^{-1,(\nu)}(V_{b'}^{(\nu)} - \hat{V}_{b'}^{(\nu)}), \tag{26}$$

TABLE I. The constraints of $\tau_{\rm NL}, g_{\rm NL}$ with $\Delta L = 150$ and $L_{\rm cut} = 800$ from different frequency combinations. The 68% C.L. is given by $\Delta\chi^2 = 2.3$ except for the last row.

Frequency combination	$\tau_{\rm NL}[\times 10^4]$	$g_{\rm NL}[\times 10^5]$
143×143	-0.7 ± 1.1	-1.8 ± 3.8
143×217	2.1 ± 1.5	-1.2 ± 4.0
$143 \times 143 + 143 \times 217$	0.4 ± 0.9	-1.2 ± 2.8
$143 \times 143 + 143 \times 217$	0	-1.4 ± 1.8

where the two free parameters are $\tau_{\rm NL}, g_{\rm NL}$, b is the index of the band, and ν is the index of the frequency combination.

We draw $\mathcal{O}(10^6)$ samples for two parameters from Monte Carlo Markov chains with flat priors $-10^6 \le \tau_{\rm NL} \le 10^6$ and $-10^7 \le g_{\rm NL} \le 10^7$. The 217 GHz map is still significantly contaminated by CIB although we use a very conservative cut which removes 40% of the sky, so we do not include 217×217 GHz in our parameter estimation. The constraints for $\tau_{\rm NL}$ and $g_{\rm NL}$ are listed in Table I. In the last row of Table I, we show the one-parameter constraint on $g_{\rm NL}$ with $\tau_{\rm NL} = 0$. For all the combinations, we find that $\tau_{\rm NL}$ and $g_{\rm NL}$ are consistent with zero (Fig. 3). We check the consistency between different frequency combinations in Fig. 4. From Fig. 4, it is seen that different bin sizes do not

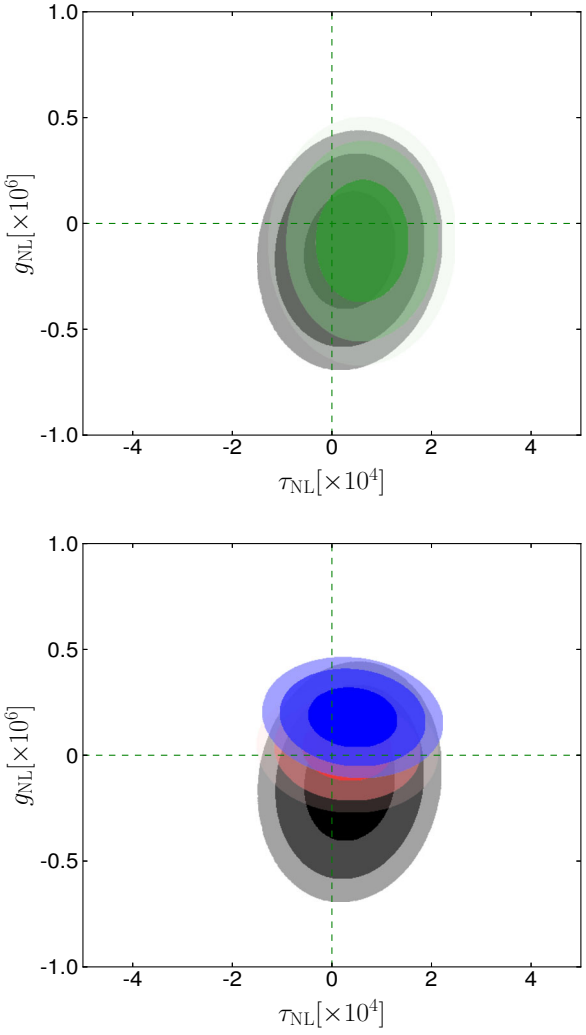

FIG. 4 (color online). The 68%, 95% and 99% confidence levels for the combination $143 \times 143 + 143 \times 217$ with different bin sizes (top) and $L_{\rm cut}$ (bottom) are indicated by the transparency of the contours. In the top panel, for $\Delta L = 150$, the contour is shown in black and green for $\Delta L = 200$. For both cases, $L_{\rm cut} = 800$. In the bottom panel, $L_{\rm cut} = 800$ is shown in black, $L_{\rm cut} = 850$ in red, $L_{\rm cut} = 900$ in blue. In these cases $\Delta L = 150$.

TABLE II. The constraints of $\tau_{\rm NL}, g_{\rm NL}$ with different ΔL and $L_{\rm cut}$ for the combination $143\times143+143\times217$. The 68% C.L. is given by $\Delta\chi^2=2.3$.

$143\times143+143\times217$	$\tau_{\rm NL}[\times10^4]$	$g_{\rm NL}[\times10^5]$
$[\Delta L=150, L_{\rm cut}=800]$	0.4 ± 0.9	-1.2 ± 2.8
$[\Delta L=150, L_{\rm cut}=850]$	0.3 ± 0.9	0.3 ± 1.4
$[\Delta L=150, L_{\rm cut}=900]$	0.4 ± 0.9	1.8 ± 1.4
$[\Delta L=200, L_{\rm cut}=800]$	0.6 ± 0.9	-0.8 ± 2.9

change the results. We also check the impact of the effective L range on the parameters. From Fig. 4, we find that adding more L range can result in a higher value of $g_{\rm NL}$ and the possible interpretation is that the small-scale non-Gaussian structures of unresolved point sources and CIB beyond the foreground mask could result in a non-negligible trispectrum at high L. All the results shown in Fig. 4 are summarized in Table II.

V. SUMMARY

We presented the first joint constraints on $\tau_{\rm NL}, g_{\rm NL}$ using Planck kurtosis power spectra that trace square temperature-square temperature and cubic temperature-temperature power spectra. The Gaussian biases in these statistics were corrected for with simulations and we made use of non-Gaussian simulations to test our pipeline. We found the best joint estimate of the two parameters to be $\tau_{\rm NL}=(0.4\pm0.9)\times10^4$ and $g_{\rm NL}=(-1.2\pm2.8)\times10^5$. If $\tau_{\rm NL}=0$, $g_{\rm NL}=(-1.4\pm1.8)\times10^5$.

ACKNOWLEDGMENTS

A. C. and C. F. acknowledge support from NSF Grant No. AST-1313319 and the James B. Ax Family Foundation through a grant to the Ax Center for Experimental Cosmology. D. R. acknowledges support from the Science and Technology Facilities Council [Grant No. ST/L000652/1] and from the European Research Council [ERC Grant Agreement No. 308082].

[1] A. H. Guth, Phys. Rev. D **23**, 347 (1981).
[2] A. D. Linde, Phys. Lett. **108B**, 389 (1982).
[3] A. Albrecht and P. J. Steinhardt, Phys. Rev. Lett. **48**, 1220 (1982).
[4] A. H. Guth, Phys. Rev. D **23**, 347 (1981).
[5] J. M. Bardeen, Phys. Rev. D **22**, 1882 (1980).
[6] C. T. Byrnes, K. Enqvist, and T. Takahashi, J. Cosmol. Astropart. Phys. 09 (2010) 026.
[7] K. T. Engel, K. S. M. Lee, and M. B. Wise, Phys. Rev. D **79**, 103530 (2009).
[8] X. Chen, B. Hu, M.-x. Huang, G. Shiu, and Y. Wang, J. Cosmol. Astropart. Phys. 08 (2009) 008.
[9] L. Boubekeur and D. H. Lyth, Phys. Rev. D **73**, 021301 (2006).
[10] E. Komatsu *et al.*, arXiv:0902.4759.
[11] A. P. S. Yadav and B. D. Wandelt, Phys. Rev. Lett. **100**, 181301 (2008).
[12] K. M. Smith, L. Senatore, and M. Zaldarriaga, J. Cosmol. Astropart. Phys. 09 (2009) 006.
[13] E. Komatsu *et al.*, Astrophys. J. Suppl. Ser. **192**, 18 (2011).
[14] J. Smidt, A. Amblard, P. Serra, and A. Cooray, Phys. Rev. D **80**, 123005 (2009).
[15] P. A. R. Ade *et al.* (Planck Collaboration), Astron. Astrophys. **571**, A24 (2014).
[16] W. Hu, Phys. Rev. D **64**, 083005 (2001).
[17] T. Suyama, T. Takahashi, M. Yamaguchi, and S. Yokoyama, J. Cosmol. Astropart. Phys. 06 (2013) 012.
[18] J. Smidt, A. Amblard, C. T. Byrnes, A. Cooray, A. Heavens, and D. Munshi, Phys. Rev. D **81**, 123007 (2010).
[19] D. Munshi, A. Heavens, A. Cooray, J. Smidt, P. Coles, and P. Serra, Mon. Not. R. Astron. Soc. **412**, 1993 (2011).
[20] J. Smidt, A. Amblard, A. Cooray, A. Heavens, D. Munshi, and P. Serra, arXiv:1001.5026.
[21] T. Sekiguchi and N. Sugiyama, J. Cosmol. Astropart. Phys. 09 (2013) 002.
[22] J. R. Fergusson, D. M. Regan, and E. P. S. Shellard, arXiv:1012.6039.
[23] D. Regan, M. Gosenca, and D. Seery, J. Cosmol. Astropart. Phys. 01 (2015) 013.
[24] N. Kogo and E. Komatsu, Phys. Rev. D **73**, 083007 (2006).
[25] T. Okamoto and W. Hu, Phys. Rev. D **66**, 063008 (2002).
[26] D. M. Regan, E. P. S. Shellard, and J. R. Fergusson, Phys. Rev. D **82**, 023520 (2010).
[27] P. A. R. Ade *et al.* (Planck Collaboration), Astron. Astrophys. **571**, A16 (2014).
[28] http://www.mpa-garching.mpg.de/komatsu/CRL/nongaussianity/localform/.
[29] M. Liguori, A. Yadav, F. K. Hansen, E. Komatsu, S. Matarrese, and B. Wandelt, Phys. Rev. D **76**, 105016 (2007).
[30] R. Pearson, A. Lewis, and D. Regan, J. Cosmol. Astropart. Phys. 3 (2012) 011.
[31] D. Munshi, P. Coles, A. Cooray, A. Heavens, and J. Smidt, Mon. Not. R. Astron. Soc. **410**, 1295 (2011).
[32] http://planck.mpa-garching.mpg.de/cmb/fnl-simulations/.
[33] P. A. R. Ade *et al.* (Planck Collaboration), Astron. Astrophys. **571**, A17 (2014).
[34] P. A. R. Ade *et al.* (Planck Collaboration), Astron. Astrophys. **571**, A6 (2014).